J. Fluid Mech. (1986), *vol.* 168, *pp.* 431–456
Printed in Great Britain

On the stability and the numerical solution of the unsteady interactive boundary-layer equation

By O. R. TUTTY†

Department of Applied Mathematics and Theoretical Physics, Silver Street, Cambridge CB3 9EW

AND S. J. COWLEY‡

Department of Mathematics, University College London, Gower Street, London WC1E 6BT

(Received 9 April 1985 and in revised form 8 January 1986)

By means of a high-frequency analysis it is shown that a Rayleigh instability is possible *within* the interactive boundary-layer formulation. This instability reflects the tendency of large-Reynolds-number flows to be unstable. For most, but not all, pressure-displacement relations both Rayleigh's and Fjørtoft's theorems hold, although Fjørtoft's criterion is not a sufficient condition for instability. However, for two pressure-displacement relations neither theorem could be proved, and for one of these, unstable flows exist which are free of inflexion points. Analytically, the existence of this instability may result in a finite-time singularity, while numerically the presence of Rayleigh modes often leads to accuracy problems which cannot be overcome by simple grid refinement. A test integration resulted in the generation of small grid-dependent eddies. It is suggested that the instability may be a possible cause of the eddy splitting observed in experiments on unsteady flows through distorted channels. This Rayleigh instability is also possible within the 'inverse' boundary-layer formulation, but is absent from classical boundary-layer problems.

1. Introduction

The emergence of interactive boundary-layer theory in recent years has resulted in asymptotic descriptions of separation and related phenomena (e.g. Stewartson 1981; Smith 1982*a*). Comparisons between *steady* large-Reynolds-number asymptotic solutions, numerical solutions of the Navier–Stokes equation and experiments have been favourable down to surprisingly low Reynolds numbers (e.g. Jobe & Burggraf 1974; Sobey 1980; Dennis & Smith 1980). However, at larger Reynolds numbers these steady asymptotic solutions generally diverge from the corresponding experimentally observed flows as a result of fluid flow instabilities.

Paradoxically there is often a close connection between steady interactive boundary-layer calculations and the large-Reynolds-number asymptotic instability analysis for related flows. For instance, essentially the same asymptotic structure describes both steady flow through a slightly distorted channel and the growth/decay of lower branch Tollmien–Schlichting (T–S) waves in unperturbed plane Poiseuille flow (Smith 1976*a*, 1979*a*). Steady asymptotic solutions are therefore often obtained by *suppressing* instabilities. Such a procedure may appear unsatisfactory at first sight, but the

† Present address: Department of Aeronautics and Astronautics, The University, Highfield, Southampton SO9 5NH.

‡ Present address: Department of Mathematics, Imperial College of Science and Technology, Huxley Building, 180 Queen's Gate, London SW7 2BZ.

agreement at stable Reynolds numbers between Navier–Stokes solutions and the large-Reynolds-number asymptotic theory gives credibility to this device. Naturally, asymptotic solutions so obtained can hold only at Reynolds numbers less than the supposedly large (but usually finite) critical value for flow instability.

Similarly, *unsteady* asymptotic solutions have been found by suppressing instabilities. For example, in Appendix A it is shown that the much-studied boundary-layer solution for unsteady flow past an impulsively started cylinder is obtained by excluding a number of rapidly growing asymptotic instabilities not contained within the classical boundary-layer formulation. Nevertheless, good agreement has been found between theory and 'low-noise' experiments at moderately large Reynolds numbers. This problem also illustrates the important point that it is sometimes not possible, nor desirable, to suppress all instabilities; in particular, Cowley, Hocking & Tutty (1985) have shown that once a point of zero shear develops in the velocity profile, a linear viscous instability, which may be the trigger for unsteady separation, arises within the classical boundary-layer formulation.

The existence of instabilities, and the decision of when and when not to include them, complicates the asymptotic study of unsteady flows compared with steady ones. In order to understand time-dependent flows a knowledge of the instabilities present in various asymptotic formulations is therefore helpful. The aim of this paper is to identify a Rayleigh instability within the unsteady interactive boundary-layer formulation, and to examine the consequences of this.

The motivation for the work arose from the experiments by Stephanoff *et al.* (1983) on flow along a channel with an asymmetric oscillating constriction. In the vicinity of the distortion the flow was laminar, the Reynolds number relatively large (i.e. between 300 and 700), and the Strouhal number small (i.e. between 0.003 and 0.07). One way of modelling this flow is to pose an interactive unsteady boundary-layer problem (§2).

In §3 we show that for this and other interactive formulations once the underlying constant shear has been sufficiently deformed a rapidly growing Rayleigh instability may arise. This instability is found to be possible both in interactive boundary-layer formulations that admit T–S waves *and* in those that do not. It results in the development of short-scale disturbances within the boundary layer; an effect not dissimilar to the inflexion-point 'spike' instabilities that are observed to develop on T–S waves (e.g. Klebanoff, Tidstrom & Sargent 1962). The same type of Rayleigh instability is also possible within the 'inverse' boundary-layer formulation (Appendix D), but is absent from classical boundary-layer problems. Similar Rayleigh modes occur in unsteady nonlinear critical layers once the constant-shear basic state has been modified by the rolling-up of vorticity within the 'cats-eyes' (Killworth & McIntyre 1985).

In order to show that the Rayleigh instability is more than a theoretical possibility, we solve the appropriate eigenvalue problem for a number of steady velocity profiles. This is done using a quadrature routine which accurately evaluates singular integrals from data provided at discrete points (see Appendix B). Then in §§4 and 5 we demonstrate that the presence of Rayleigh modes leads to accuracy difficulties in the numerical integration of the unsteady interactive boundary-layer equations. The finite-difference scheme used is based on Cebeci's (1979, 1983) extension of the standard Keller-box method. The scheme is second-order accurate, and allows backflow. The calculations were stable where there were no Rayleigh modes, and unstable where such modes existed.

2. Formulation and initial discussion

Our interest in flow along a channel with an oscillatory constriction led us to study the family of flows generated by vertically moving surfaces. The generic formulation of the interactive boundary-layer problem for such flows is

$$u_t + uu_x + vu_y = -p_x + u_{yy}, \quad u_x + v_y = 0, \tag{2.1a, b}$$

$$u \to y \quad \text{as } x \to -\infty, \tag{2.1c}$$

$$u = 0, \quad v = f_t \quad \text{on } y = f(x,t), \tag{2.1d}$$

$$u \to y + A(x,t) \quad \text{as } y \to \infty, \tag{2.1e}$$

where (x, y) are the streamwise and transverse Cartesian coordinates respectively, (u, v) are the corresponding velocity components, t is time, p is the pressure, f gives the position of the surface, and A is the displacement function. The unsteady Prandtl transform

$$y \to y + f(x,t), \quad v \to v + uf_x + f_t, \tag{2.2}$$

leaves (2.1 *a–c*) unchanged, while the boundary conditions (2.1 *d*, *e*) are simplified to

$$u = v = 0 \quad \text{on } y = 0, \tag{2.3a}$$

$$u \to y + A + f \quad \text{as } y \to \infty. \tag{2.3b}$$

To close the problem, a 'pressure-displacement relation' or 'interaction law' must be specified. For subsonic, supersonic, hypersonic, Smith–Daniels (S–D) and jet-like boundary-layer flow over small distortions these relations are respectively

$$p(x,t) = \frac{1}{\pi}\int_{-\infty}^{\infty} \frac{A_\zeta(\zeta,t)}{x-\zeta}\,\mathrm{d}\zeta, \quad p = -A_x, \quad p = -A, \quad p = A, \quad p = -A_{xx} \tag{2.4a–e}$$

(e.g. Stewartson 1981; Smith 1982*a*; Smith & Daniels 1981). Equation (2.4*c*) also applies to certain free-surface flows (Gajjar & Smith 1983).

The expressions (2.4*a–e*) hold for flows over distortions with appropriate interactive lengthscales. For much shorter humps they reduce to

$$A = 0, \tag{2.4f}$$

which also applies to Poiseuille flow through both symmetrically distorted plane channels (Smith 1976*a*) and axisymmetrically distorted circular pipes (Smith 1976*b*).†

The interactive formulation for plane Poiseuille flow through asymmetrically deformed channels depends on the length of the distortion, λ. For $\lambda = O(R^{\frac{1}{7}})$, where R is the Reynolds number, the flow on both walls has to be solved simultaneously (Smith 1976*a*). The governing equations and boundary conditions in each wall layer are again (2.1 *a*, *b*, *c*) and (2.3*a*), but with (2.3*b*) replaced by

$$u_\pm \to y_\pm \mp A + f_\pm \quad \text{as } y_\pm \to \infty,$$

where the upper/lower wall is denoted by the upper/lower subscript. The two boundary layers interact through the pressure-displacement relation

$$p_+ - p_- = \frac{1}{30} A_{xx}. \tag{2.4g}$$

† Although $A = 0$ means that there is no interaction between pressure and displacement, (2.4*f*) is normally grouped with interaction laws (2.4*a–e*) because steady solutions for law (2.4*f*), like those for (2.4*a–e*), do not become singular at the onset of reversed flow.

If $\lambda \gg R^{\frac{1}{7}}$, (2.4$g$) simplifies to $p_+ = p_-$, which implies $A = \frac{1}{2}(f_+ - f_-)$. The resulting problem is equivalent to one with $A = 0$ and a forcing $f = \frac{1}{2}(f_+ + f_-)$. If $\lambda \ll R^{\frac{1}{7}}$ then the boundary layers are independent in the vicinity of the distortion, and (2.4g) reduces to $A = 0$ (Secomb 1979).

The nature of solutions to (2.1)–(2.4) depends on whether or not there are instabilities included in the formulation.† For the case of the linearized problem, analytical solutions show that the stability of the underlying shear flow, $u = y$, to T–S waves has an important qualitative effect on the solution. Three different types of behaviour can be identified:

(i) For (2.4b, c, f) stable analytical solutions exist (Ryzhov & Zhuk 1982; Duck 1985a).

(ii) For (2.4a, e, h) the basic shear is unstable to 'high'-frequency T–S disturbances (Smith 1979a, b, c; Bogdanova & Ryzhov 1983). A distortion oscillated so as to excite all frequencies thus generates a growing disturbance, which for $t \gg 1$ is dominated by the fastest-growing mode (Benjamin 1961). This mode has an order-one growth rate, wavenumber and frequency.

(iii) For (2.4d) unstable T–S waves again exist, however unlike (ii) there is no fastest-growing mode. In particular for wavenumbers $\alpha \gg 1$, the growth rate $\mathrm{Im}\,(\alpha c) \sim (\frac{1}{2}\alpha)^{\frac{1}{2}}$, with the result that the problem is ill-posed. Thus, if all frequencies are initially excited, the dominant disturbance lengthscale tends to decrease as shorter-wavelength modes grow to significance. For appropriate initial conditions this results in a singularity developing within a finite time (cf. Moore 1979; also Professors S. N. Brown & F. T. Smith private communication 1984).

Instabilities are therefore often unavoidably excited for relations (2.4a, d, e, h). *Inter alia* this has important consequences for numerical calculations; for instance the inevitable errors in any numerical solution may excite spurious disturbances and lead to departures even from the exact solution $u = y, f = 0$. This effect is particularly acute for finite-difference calculations with (2.4d), because attempts to improve the accuracy by grid refinement may result only in the introduction of shorter-wavelength faster-growing numerical errors (cf. §5).

Although nonlinear effects modify the growth of any instability, for example through harmonic–harmonic interactions, numerical calculations by Duck (1985a) and others demonstrate qualitative differences in solution depending on whether growing T–S disturbances are present or not. Growth in the amplitude of T–S waves is not, however, the only way that an interactive boundary-layer calculation can become dominated by instability. In the next section we show that once the underlying constant shear has been deformed a Rayleigh instability may develop. This instability can arise for *any* of the above pressure-displacement relations. Its occurrence leads to the typical disturbance lengthscale decreasing and accuracy difficulties in numerical calculations.

3. Rayleigh modes

The Rayleigh instabilities of interest have short wavelengths and high frequencies compared with the lengthscale and oscillation frequency of the forcing. We therefore introduce the fast length and time scales $(X, T) = \alpha(x,t)$, where $\alpha \gg 1$. As usual, the

† For example, in the channel flow problem instabilities may be included/excluded by suitable choice of the distortion length.

linear stability of the exact solution, denoted by the subscript zero, is tested by introducing infinitesimal harmonic disturbances of amplitude ϵ:

$$(u, v) = (u_0, v_0)(x, y, t) + \epsilon \mathscr{A}(x, t) \exp(\mathrm{i}\Theta(X, T))(\bar{u}, \alpha\bar{v})(x, y, t) + \ldots, \quad (3.1a)$$

$$(p, A) = (p_0, A_0)(x, t) + \epsilon \mathscr{A}(x, t) \exp(\mathrm{i}\Theta(X, T))(\bar{p}, \bar{A})(x, t) + \ldots, \quad (3.1b)$$

where $$\Theta_X = K(x, t), \quad \Theta_T = -K(x, t)\, c(x, t), \quad K_t + (cK)_x = 0. \quad (3.1c)$$

$\epsilon\mathscr{A}$, αK and c are the local amplitude, wavenumber and complex wavespeed respectively, and should strictly be expanded in powers of $\alpha^{-\frac{1}{8}}$ (although that is not done here as the calculation is taken only to leading order). Hereafter the dependence of variables on the slow scales x, t will not be displayed explicitly.

Substitution of (3.1) into (2.1) yields the long-wave Rayleigh (LWR)† equation at leading order:

$$\mathrm{i}K\bar{u} + \bar{v}_y = 0, \quad \mathrm{i}K(u_0 - c)\,\bar{u} + \bar{v}u_{0y} = -\mathrm{i}K\bar{p}. \quad (3.2a, b)$$

The boundary conditions are the inviscid ones of zero velocity normal to the wall and a match with the displacement function at infinity, i.e.

$$\bar{v} = 0 \quad \text{on } y = 0, \quad \bar{u} = \frac{-\bar{v}_y}{\mathrm{i}K} \to \bar{A} \quad \text{as } y \to \infty. \quad (3.3a, b)$$

The no-slip boundary condition can be satisfied by introducing a thin passive Stokes layer of thickness $\alpha^{-\frac{1}{8}}$ adjacent to the wall.

A solution to (3.2) and (3.3) exists if

$$\bar{A} = -\bar{p} \int_0^\infty (u_0 - c)^{-2}\, \mathrm{d}y. \quad (3.4)$$

If $u_0 = c$ at some $y = y_c$, the integral is to be evaluated with $\mathrm{Im}(c) = 0+$.

Substitution of (3.1*b*) into the pressure-displacement relations of §2 yields

$$\bar{A} = -s\bar{p}, \quad (3.5)$$

where $s = 0$ for (2.4*a*, *b*, *e*, *f*, *h*), $s = 1$ for (2.4*c*) and $s = -1$ for (2.4*d*). The eigenvalue relation for the complex wavespeed c is therefore

$$\int_0^\infty \frac{1 - u_{0y}}{(u_0 - c)^2}\, \mathrm{d}y - \frac{1}{c} = s, \quad (3.6)$$

where the integral has been written in a form suitable for numerical integration ($u_{0y}(y)$ usually tends to unity exponentially as $y \to \infty$). Once c is determined from (3.6) the variations in local wavenumber and growth rate can be calculated from (3.1*c*).

To show the existence of realistic velocity profiles for which (3.6) can be satisfied, we consider flow past the distortion

$$f(x, t) = h(t) \exp\left(\frac{-x^2}{A}\right). \quad (3.7)$$

For simplicity the 'zero-displacement' interaction law (2.4*f*) is studied; without loss of generality we can then choose the normalization $A = \frac{1}{10}$. In the case of flows through channels, symmetric distortions, or those much longer or shorter than $R^{\frac{1}{8}}$, are therefore being considered (see §2).

† We emphasize that while the disturbance wavelength is *short* compared with the lengthscale of the forcing, it is large compared with the boundary-layer thickness. The latter is the characteristic wavelength of Rayleigh modes, thus the *long*-wave Rayleigh equation is obtained.

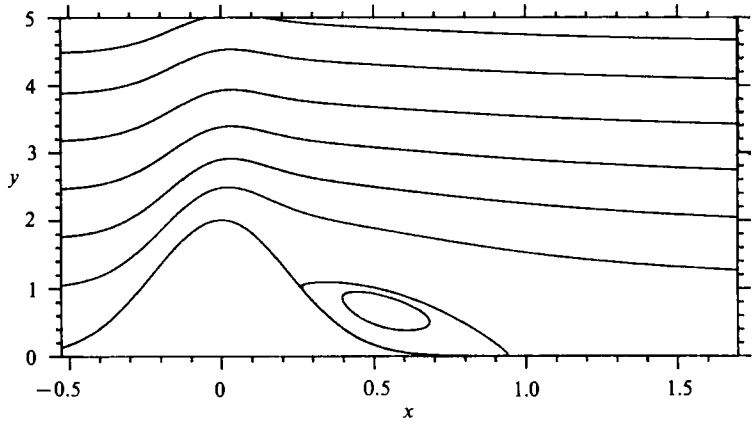

FIGURE 1. Streamline pattern for steady flow past contraction (3.7) with $h = 2$.

Relation (2.4f) has the advantage over other interaction laws that there are no upstream free-interactions (Smith 1976a), and hence a shorter integration range in x is adequate. Further, the choice $A = 0$ means that streamlines far from the wall are not significantly deflected, i.e. $A = 0$ is similar, but *not* identical, to putting a 'lid' on the flow (cf. flows with other interaction laws where the flow tends to lift up over the distortion, e.g. Smith 1982a). As a result the fluid tends to accelerate over the hump, which means, when combined with the reduction in shear near the wall, that an inflexion point is likely to develop away from the wall.

The stability of steady flows is considerd first (see §§4 and 5 for unsteady flows). Numerical solutions of (2.1)–(2.3) for steady forced states were obtained using the Keller-box method (Smith 1974), together with extended backward differences in regions of reversed flow (Dijkstra 1979). The streamline pattern for a hill of height $h = 2$ is illustrated in figure 1.

There are objections to using extended backwards differences to deal with backflow, as pointed out by Smith (1984). A more satisfactory alternative method is to find the steady solution as the large-time limit of an unsteady flow (Rizzetta, Burggraf & Jenson 1978), but a comparison between the two methods for $h = -2$ yielded solutions which were graphically indistinguishable. Consequently, we do not believe that our subsequent stability calculations are adversely affected by using the computationally cheaper, extended-backward-difference method. Further, the unsteady time-marching method may not lead to the steady solution if LWR modes exist. This is demonstrated in §5 where converged steady solutions are integrated forward in time without changing the hill height. Any LWR modes present magnify the unavoidable small numerical errors and an instability rapidly develops (see figure 3).

Given a steady velocity profile, solutions to (3.6) were sought by the secant method. The only significant difficulty was in evaluating the integral when $|\mathrm{Im}\,(c)| \ll 1$, and this was overcome by using a rational function of polynomials to approximate the integrand locally (see Appendix B). The resulting Padé-approximant method accurately evaluates contour integrals around single or double poles, even when the integrand is known only at discrete grid points.

For $h = 2$ unstable eigensolutions could be found from $x = x_{\mathrm{L}}$, where $x_{\mathrm{L}} \approx 0.05$ is shortly after the peak of the hill, to $x = x_{\mathrm{U}} \approx 2.4$. The complex wavespeeds for $x_{\mathrm{L}} < x < x_{\mathrm{U}}$, which were obtained from calculations based on a rectangular grid

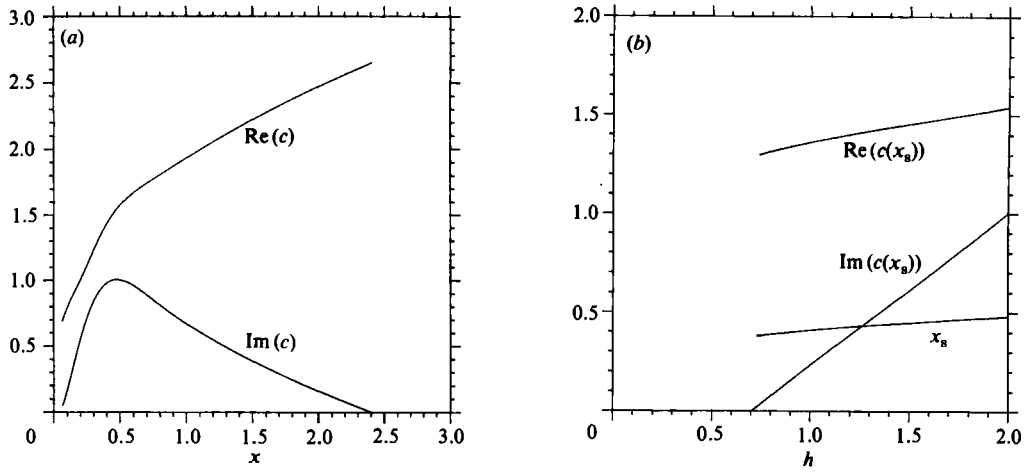

FIGURE 2. (*a*) Complex wavespeed c as a function of x for flow illustrated in figure 1. (*b*) Maximum value of Im (c) for different distortion heights. Also plotted are the corresponding Re (c), and the position $x = x_s$ of the maximum.

with $y_{\max} = 5$ and x and y steps of 0.0125 and 0.05 respectively, are illustrated in figure 2(*a*). The growth-rate tends to zero at x_L, x_U. The values of c found with the grid steps doubled are graphically indistinguishable from those shown in figure 2(*a*). As the height of the hill is reduced the range of x for which the LWR instability exists decreases, as does the maximum value of Im (c) (figure 2*b*). LWR modes were found for $h \gtrsim 0.70$, and the flow was unidirectional for $h \lesssim 1.51$; thus reversed flow is not a requisite for this instability. Similar stability calculations have also shown that LWR modes can be found for steady flow over a periodic distortion when the subsonic law (2.4*a*) applies.

For all distortions solved with $h > 0$, Fjørtoft's criterion is satisfied downstream of an h-dependent point on the lee side of the hill (i.e. $u_{0yy}(y)(u_0(y) - u_0(y_s)) < 0$ for some y, where $u_{0yy}(y_s) = 0$). Thus for distortion (3.7), satisfaction of Fjørtoft's criterion is not sufficient for LWR modes to exist.

Fjørtoft's criterion is however a *necessary* condition for the instability of flows with the disturbance boundary condition $\overline{A} = 0$, i.e. $s = 0$; for proceeding in the standard way from (3.2*a*, *b*) it follows that (e.g. Drazin & Reid 1981)

$$\int_0^y \left(|\bar{v}_y|^2 + \frac{u_{0yy}|\bar{v}|^2}{u_0 - c} \right) \mathrm{d}y' = [\bar{v}^* \bar{v}_y]_0^y, \tag{3.8}$$

where * denotes a complex-conjugate. If $\overline{A} = 0$, as is the case for interaction laws (2.4*a*, *b*, *e*–*h*), it follows from (3.3) that the right-hand side is zero in the limit $y \to \infty$. Rayleigh's inflexion-point theorem and Fjørtoft's necessary criterion for instability then result from taking the real and imaginary parts of (3.8) respectively.

However if $\overline{A} = \pm \overline{p}$ (see 2.4*c*, *d*)) the right-hand side of (3.8) is *non-zero* as $y \to \infty$. In Appendix C it is shown that (i) Rayleigh's theorem is then replaced by the condition that that u_{0yy} must be positive somewhere in the flow, and (ii) that for (2.4*d*), unstable velocity profiles exist which are inflexion-point free.

The analysis leading to the eigenvalue relation (3.6) is based on $\alpha \gg 1$, i.e. a typical disturbance wavelength is assumed short compared with the interaction lengthscale. However, α cannot be made too large without neglected physical effects coming to the fore. In particular, disturbances with wavelengths of the same order as the

asymptotically small boundary-layer thickness are governed by the full Rayleigh equation:

$$(u_0 - c)(\bar{v}_{yy} - k^2\bar{v}) - u_{0yy}\bar{v} = 0, \tag{3.9}$$

where k is a suitably scaled wavenumber (see also Smith & Bodonyi 1985). For flows with interaction laws (2.4a, b, e, f, h) the boundary conditions are $\bar{v} = 0$ on $y = 0$ and $\bar{v} \to 0$ as $y \to \infty$.

Smith & Bodonyi (1985) have solved (3.9) for both model analytical velocity profiles and numerically generated ones. They found that as the height of the distortion increased the flow became unstable first to small k, i.e. LWR, modes, and that there was a cutoff value of k above which unstable modes could not be found. Independently, we obtained similar results using a family of piecewise-linear profiles with a constant shear at infinity†; but in addition profiles were found for which unstable modes with only non-zero wavenumbers existed. Solutions to (3.9) show that for $k = O(1)$ Fjørtoft's criterion is again not a sufficient instability condition for velocity profiles that tend to a constant shear at infinity. In contrast, for classical boundary-layer velocity profiles, i.e. profiles which tend to a constant velocity as $y \to \infty$, it is generally accepted that Fjørtoft's condition is sufficient (Tollmien 1936, and others).

There is another important difference between the Rayleigh modes associated with interactive velocity profiles and those for classical boundary-layer profiles. For $k \ll 1$ the above implies that the 'interactive' LWR modes have Im (c) formally comparable to Re (c), i.e. the growth-rate is a leading-order effect. It is for this reason that the LWR instability is contained within the interactive boundary-layer formulation. However, for classical velocity profiles the Rayleigh growth rate is a second-order effect, i.e. Im (c) $\ll$ Re (c) when $k \ll 1$. As a result the classical unsteady boundary-layer formulation does not include an inherent LWR instability.‡

The unsteady 'inverse' boundary-layer problem has also received attention recently (Cebeci 1983). In this formulation the boundary conditions (2.1d, e), and the interaction law are replaced by

$$u = v = 0 \text{ on } y = 0,\ u \to U \text{ as } y \to \infty, \quad \delta(x,t) = \int_0^\infty \left(1 - \frac{u}{U}\right) \mathrm{d}y \tag{3.10}$$

respectively, where $\delta(x,t)$ is a specified displacement thickness. A stability analysis demonstrates that unstable LWR modes are again possible if the velocity profile contains an inflexion point (see Appendix D).

In the next two sections the effects of unstable LWR modes on a numerical integration of the interactive boundary-layer equation are illustrated.

4. Numerical method

The unsteady interactive boundary-layer equation has previously been integrated numerically by Ruban (1978), Rizzetta *et al.* (1978) and Duck (1979, 1985a, b). Duck (1979) used a second-order Keller-box scheme, and this is the method we adopt where

† Profiles with three linear components were used. As a check on this crude approximation, solutions of (3.9) were also calculated for piecewise-linear boundary-layer profiles that tend to a constant velocity at infinity. The Rayleigh stability characteristics so obtained were in good qualitative agreement with the known results for similarly shaped smooth velocity profiles.

‡ With $\bar{A} = 0$ in (3.3b) and $u_{0y} \to 0$ as $y \to \infty$, (3.2) and (3.3) yield the eigensolution $c = 0$, $\bar{p} = 0$, and $\bar{v} = \beta u_0$, where β is a constant. Hence at leading order the solution is neutral, although at higher order it turns out to be a decaying T–S wave.

$u > 0$. However, Cebeci (1979) found that the straightforward Keller-box method was inadequate when extended regions of backflow developed. To overcome this he introduced a 'zigzag' finite-difference molecule in regions of reversed flow. This method allows upstream influence, but iterates forward in the x-direction throughout the calculation. It has been used with success in a number of boundary-layer problems (Cebeci 1979, 1983), and is relatively straightforward to incorporate into Duck's (1979) interactive code. Only an outline of the method is given here.

The solution was found on a finite-difference grid (x_i, y_j, t_k), where x_0 is the farthest point upstream,

$$(y_0, t_0) = (0, 0), \quad (x_i, y_j, t_k) = (x_{i-1}, y_{i-1}, t_{k-1}) + (\Delta x_i,\ \Delta y_j, \Delta t_k), \tag{4.1}$$

for i, j, k from $1, 2, \ldots$ to I, J, K respectively. The finite-difference equations were derived by first writing the governing equations (2.1) as a first-order system in terms of the new dependent variables $G(x, y, t)$, $C(x, y, t)$, and $E(x, y, t)$, where G is the stream function and

$$C = G_y, \quad E = C_y. \tag{4.2}$$

These two equations were approximated by second-order centre differences and averages about the point $(x_i, y_{j-\frac{1}{2}}, t_k)$, while the standard Keller-box method centred on $(x_{i-\frac{1}{2}}, y_{j-\frac{1}{2}}, t_{k-\frac{1}{2}})$ was applied to the momentum equation where the streamwise flow u was positive. At points with reversed flow a mid-point $(x_i, y_{j-\frac{1}{2}}, t_{k-\frac{1}{2}})$ was taken, and the x-derivatives were approximated by a weighted zigzag average of the centre-differenced formulae at $(x_{i-\frac{1}{2}}, y_{j-\frac{1}{2}}, t_k)$ and $(x_{i+\frac{1}{2}}, y_{j-\frac{1}{2}}, t_{k-1})$. For a constant x-step the arithmetic mean retains second-order accuracy.

In order to reduce the calculation time for the exponential hill (3.7), the transformation

$$x = \sinh(\zeta) \tag{4.3a}$$

was employed. Second-order accuracy is preserved by use of a constant ζ-step. Where increased accuracy near the wall was necessary, a variable y-step was implemented by means of the transformation

$$y = z + \mu z^3, \tag{4.3b}$$

where μ is a constant.

Further details of the numerical solution procedure, including the Newton iteration which deals with the nonlinearity, can be found in Cebeci (1979, 1983), Bradshaw, Cebeci & Whitelaw (1981) and Smith (1974). The iteration procedure was to make one complete sweep in the x-direction at each time step, and at each x-station repeat the local iteration until

$$\sum_m |\delta_m| < 10^{-10}, \tag{4.4}$$

where the δ_m were the changes to the numerical values of the dependent variables at each iteration. The zigzag molecule only allows information to travel upstream at the rate of one grid point per time step, hence it is necessary that $|u| \Delta t < \Delta x$ wherever $u < 0$ if sufficient upstream influence is to be accounted for. This condition was satisfied in all the results presented below.

The zero-displacement law (2.4f) was again chosen for study; the subsonic problem can also be solved after modifications to the above scheme (Veldman & Dijkstra 1980 give a finite-difference approximation for (2.4a)). However, the other interaction laws both relate the pressure to the displacement at a point and admit upstream influence. We have found that this combination leads to difficulties in formulating a convergent numerical scheme based on local finite differences, even after allowing for a degree of upstream influence through use of a zigzag molecule for the interaction law. In

particular, such schemes appear divergent when applied to the supersonic problem, and it seems necessary to allow the displacement function to interact instantaneously over the whole x-range. Both the semi-implicit finite-difference scheme of Rizzetta *et al.* (1978) and the spectral codes of Burggraf & Duck (1982), Duck (1985*a*) achieve this.

If the wall starts moving at $t = 0$ then the boundary-layer thickness is proportional to $t^{\frac{1}{2}}$ for $t \ll 1$. To improve accuracy during this initial diffusive growth, we introduce the similarity variables (cf. Cebeci 1979)

$$\tau = (\beta t)^{\frac{1}{2}}, \quad \eta = y(\beta t)^{-\frac{1}{2}} = y\tau^{-1}. \tag{4.5}$$

The transformation of the dependent variables and governing equations is straightforward and the details are omitted. The changeover between the similarity variables used at the start of the calculation and the variables (G, C, E, p) used subsequently was made at $\tau = 1$. With this choice there is no need to interpolate between grid points in the η- and y-coordinates (see (4.5)).

Below, unless specifically mentioned, a reference to Δy will imply that $\mu = 0$ with $y_{\max} = 5.0$ in (4.3*b*), and to Δz, that $\mu = 3.0$ with $y_{\max} = 4.0$.

5. Results

As a check on the codes, and to investigate for instabilities, the steady solutions for flows past hills of shape (3.7) were taken as the initial conditions for unsteady integrations with a fixed hill height. In all the tests for which *sufficiently refined* grids were used, instabilities developed if and only if LWR modes had been found in §3. For example, with $h = 0.6$ no LWR modes were found (figure 2), and no instabilities were evident in the unsteady integrations. Similarly, with a hill height for which the steady solution satisfies Fjørtoft's criterion nowhere ($h = -2$), unsteady integrations converged to a steady state. The latter case provides an example where the zigzag molecule successfully describes an extensive region of reversed flow. The large-time limit of the unsteady integration, which is almost identical with the steady solution of §3, also provides confirmation of the accuracy of the backwards-difference approximation of that section.

As a second check, some of Duck's (1979) calculations for flows past moving distortions were repeated. For the distortion amplitudes he considered, the flows are stable to LWR modes, and agreement was found with figures 6 and 7 of his paper.

Unsteady calculations were also performed for a steady hill with $h = 0.9$; a height for which LWR modes exist. In these runs the LWR modes so magnified the inevitable small numerical errors that a growing disturbance appeared. There is no backflow in the steady flow, and so the same exact solution satisfies both the steady and the unsteady finite-difference equations. The initial errors in the unsteady integration are thus related to the Newton iteration convergence criterion for the steady solution. The fact that the instability can develop from such small errors (typically 10^{-10}) suggests that the finite-difference scheme is modelling the equations faithfully.

A larger, and better defined, initial perturbation can be introduced by using the zigzag molecule throughout the grid for, say, the first 10 time steps. Figure 3 illustrates the growth of the pressure perturbation for a run which was started in this manner, and for which $\Delta\zeta = \Delta t = 10^{-4}$ and $\Delta z = 0.02$. Theoretically it should have been possible, given the local wavenumber, to predict the local wavespeed and growth rate from the theory of §3. Although the calculated and predicted values were always

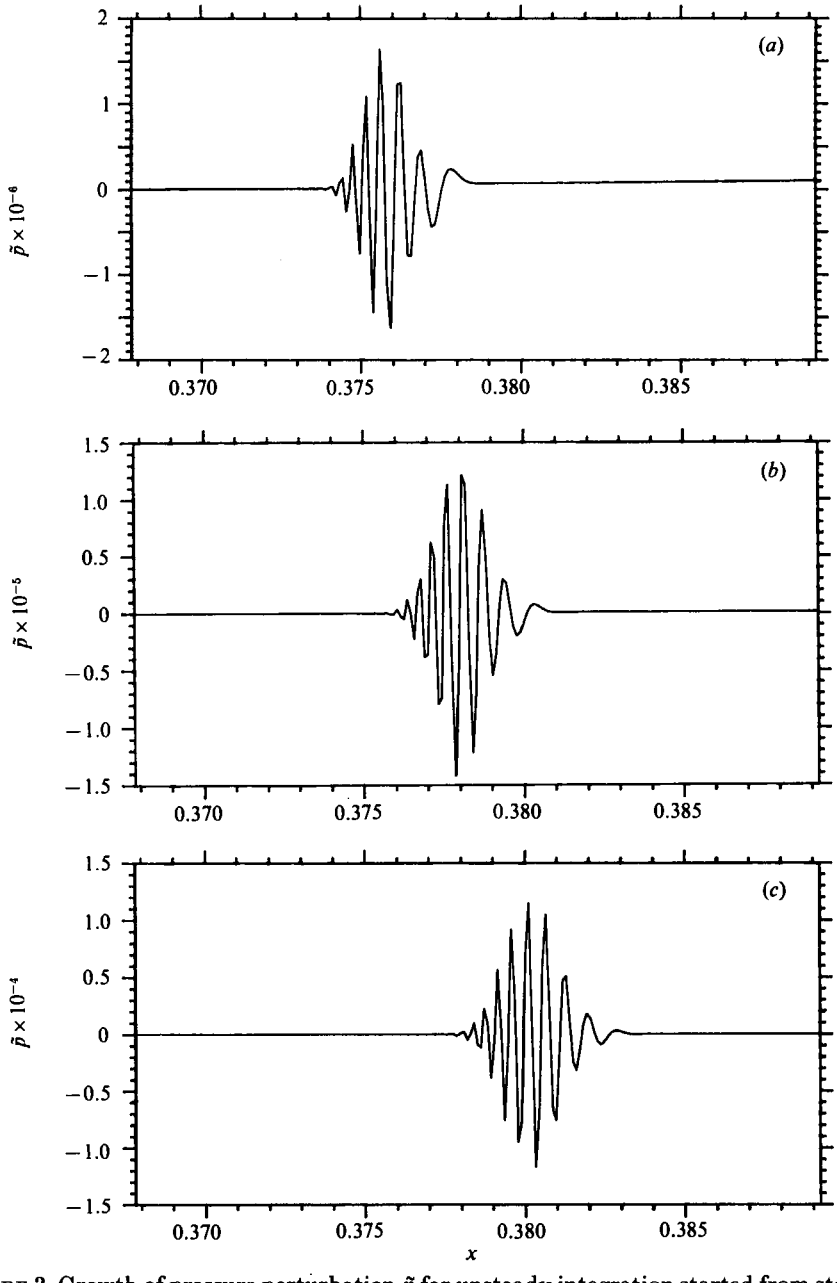

FIGURE 3. Growth of pressure perturbation $\tilde{p}$ for unsteady integration started from steady solution (constriction (3.7) with $h = 0.9$). (*a*) $t = 0.008$, (*b*) 0.010, (*c*) 0.012. The grid is $\Delta t = \Delta\zeta = 10^{-4}$ and $\Delta z = 0.02$.

of the same order, we were unable to obtain consistently good agreement. This difference may arise because the simple analysis based on our theory assumes a wavetrain with amplitude varying relatively slowly in x, whereas the disturbance shown in figure 3 may vary too rapidly. However, good agreement between the numerical calculations and the LWR instability was obtained by plotting the streamwise velocity perturbation and the amplitude of the corresponding complex

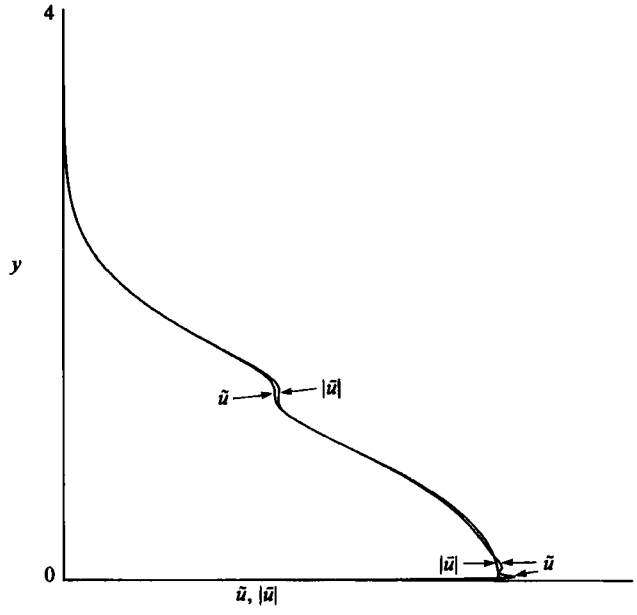

FIGURE 4. Comparison of streamwise velocity perturbation $\tilde{u}$ and calculated eigenfunction $|\overline{u}|$ for constriction (3.7) with $h = 0.9$ (normalized at $y = 0.1764$). The grid is $\Delta t = \Delta\zeta = 10^{-4}$ and $\Delta z = 0.01$ with $y = 4z^2$.

eigenfunction $\overline{u}$ (normalized to have the same value at $y = 0.1764$) – see figure 4. This graph is for a run with $\Delta z = 0.01$, $\Delta\zeta = \Delta t = 10^{-4}$, and a y-scaling, $y = 4z^2$, which ensured sufficient resolution within the thin Stokes layer at the wall. The point of zero shear perturbation in the figure is real and corresponds to the inflexion point in the steady velocity profile (see (3.4)).

The likely effect of grid refinement on the integrations can be deduced by noting that the growth rate of LWR modes is inversely proportional to the wavelength, and that in a finite-difference calculation the shortest-wavelength disturbance present will be governed by the grid size Δ. So if the numerical solution is known to an accuracy $O(E)$, where E might be a typical rounding error, the perturbation amplitude is liable to become formally order one in a time $O(-(\Delta \ln E)/\mathrm{Im}\,(c))$. Refining $\Delta\zeta$ and Δt should therefore lead to shorter-wavelength faster-growing disturbances. This trend was reflected in our calculations (see also figures 6–8), although it proved impossible to demonstrate conclusively that halving $\Delta\zeta$ and Δt exactly doubled the growth rate. Further, to the extent that computational resources were available (i.e. down to $\Delta t = \frac{1}{32}\Delta\zeta = \frac{1}{32}10^{-4}$), reducing Δt for fixed $\Delta\zeta$, Δz increased the growth rate, although not necessarily in proportion. (See below for discussion of the grid dependence for moving distortions.)

Calculations were next performed for a distortion with the time dependence

$$h(t) = 0 \quad \text{for } t < 0, \quad h(t) = H \sin^2(\tfrac{1}{2}\pi\omega t) \quad \text{for } t > 0, \tag{5.1}$$

where $\omega = 1$ was chosen as a typical frequency. First, the expansion $H = -2$ was studied. Figure 5 illustrates the wall shear at various times for a run with $\Delta\zeta = 0.025$, $\Delta t = 0.0125$, and $\Delta y = 0.1$. A significant region of backflow develops, which the code successfully describes without becoming unstable. Note that the reversed-flow eddy at the wall peaks in strength before the expansion has moved fully out, and is rapidly

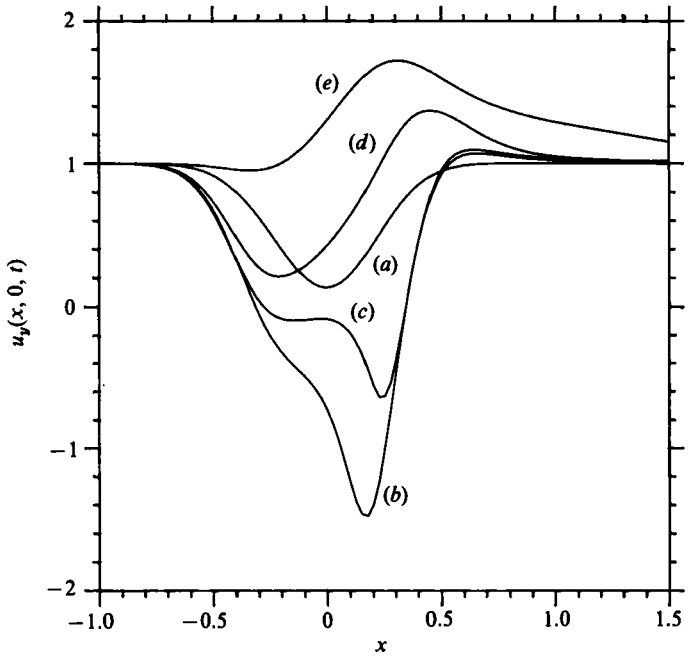

FIGURE 5. Wall shear at (*a*) $t = 0.25$, (*b*) 0.75, (*c*) 1.0, (*d*) 1.25, (*e*) 1.75, for an oscillating expansion with $H = -2$. The grid is $\Delta t = 0.0125$, $\Delta\zeta = 0.025$, and $\Delta y = 0.1$.

eliminated as the wall starts to move in again. The flow becomes almost periodic after only two complete cycles.

A similar calculation was then performed for $H = 2$, with $\Delta\zeta = 0.05$, $\Delta t = 0.0125$, $\Delta y = 0.1$, $\zeta_{\min} = -2.5$, and $\zeta_{\max} = 2.5$. As illustrated in figure 6 an eddy is generated on the lee side of the hump as the wall moves out. Then as the wall moves back in, this eddy splits in two with a clockwise-rotating eddy swept downstream with the flow. However, when the ζ-step is halved ($\Delta\zeta = 0.025$), rather than a smoother version of this solution being obtained, the flow structure breaks up with two, and later three, smaller eddies formed downstream of the hump (figure 7). With the ζ-step doubled ($\Delta\zeta = 0.1$) the eddy splitting is very much less pronounced – see figure 8.†

For each of the three values of $\Delta\zeta$ above, the solutions were found to become approximately independent of Δt with step refinement. For instance, for $\Delta\zeta = 0.05$ runs with $\Delta t = 0.025$, 0.0125 (figure 6), and 0.00625 yielded almost identical streamline patterns and pressures. Also, although the flow in figure 7 for $\Delta\zeta = 0.025$ changes slightly on reducing Δt (three eddies appear downstream), the streamline patterns are approximately the same for $\Delta t = \frac{1}{8}\Delta\zeta$ and $\frac{1}{16}\Delta\zeta$.

In figure 9 the Fourier spectra of the pressure for some of the runs with $\Delta\zeta = 0.025$ have been plotted (essentially the same spectra were obtained using 32-figure arithmetic and a tighter iteration tolerance than (4.5)). In order to remove the effect of the discontinuity between $\zeta_{\min}$ and $\zeta_{\max}$, which would introduce extra high-wavenumber modes, the pressure has been scaled by $\frac{1}{2}(1-\tanh(10(\zeta-4)))$. The spectra agree up to about $t = 1.25$ (although this does not necessarily imply that the numerical solution is accurate – see figure 10). For larger times a major difference in the spectra develops about wavenumber 50, where the difference between the run

† The 'kinks' in the streamlines near the wall in figures 6–8 are due to the contouring routine rather than irregularities in the calculated values of the stream function.

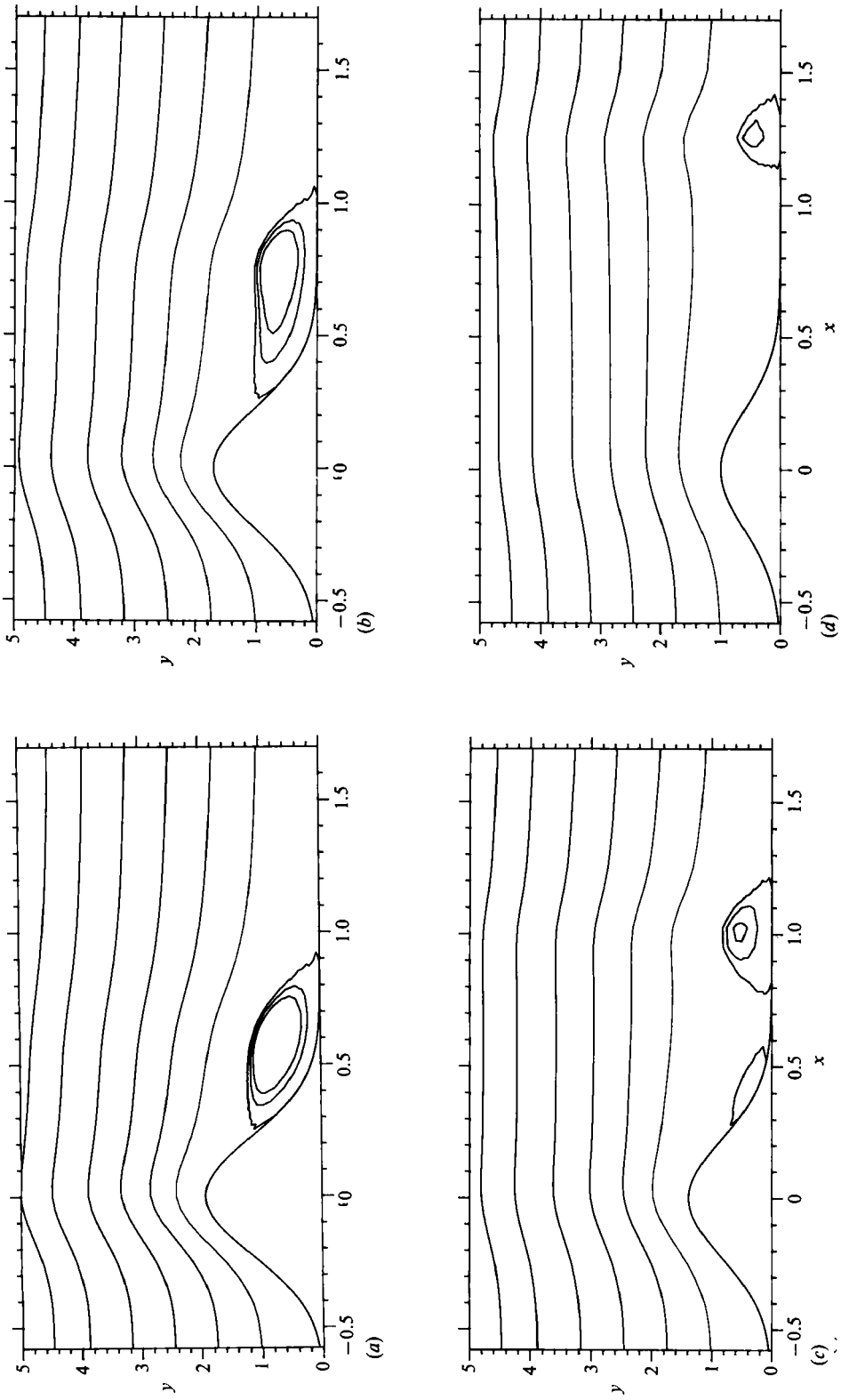

FIGURE 6. Streamline pattern for oscillating contraction with $H = 2$, $\Delta\zeta = 0.05$, $\Delta t = 0.0125$, $\Delta y = 0.1$. (*a*) $t = 1.125$, (*b*) 1.25, (*c*) 1.375, (*d*) 1.5.

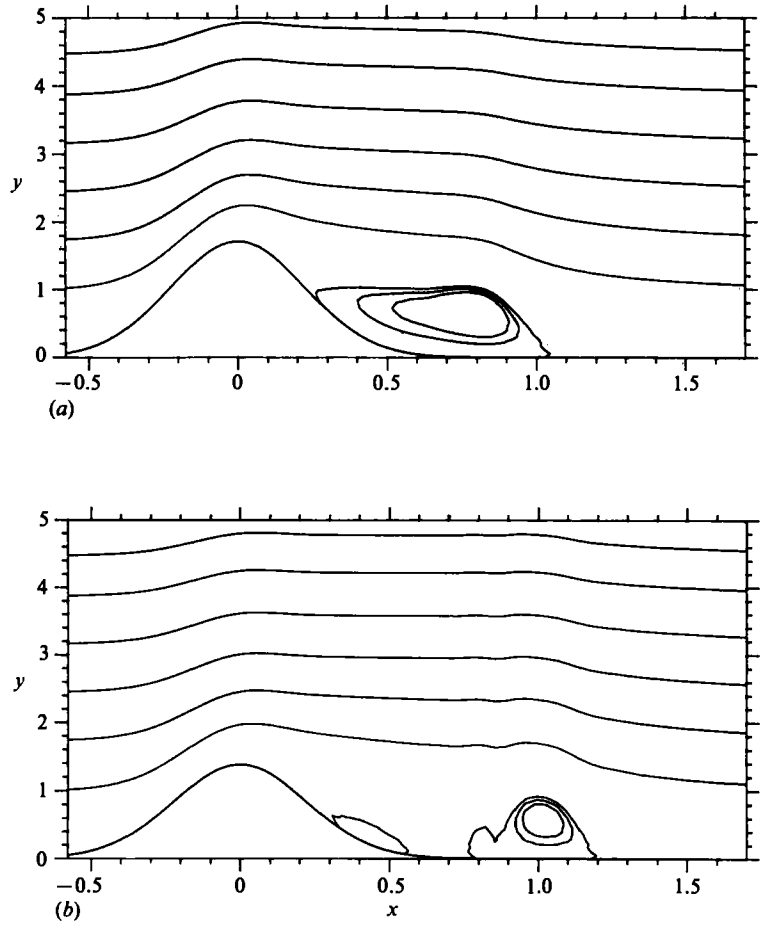

FIGURE 7. As for figure 6, but $\Delta\zeta = 0.025$ and (*a*) $t = 1.25$, (*b*) 1.375.

with $\Delta t = \Delta\zeta$ (one downstream eddy) and those with smaller Δt (several downstream eddies) is both growing in time, and increasing as Δt is decreased. This difference appears to be the 'eddy-splitting' process as it has the correct wavenumber for the approximately four $\Delta\zeta$-step wide main eddies that occur with the smaller Δt.

Next, the effect of holding Δt constant and varying $\Delta\zeta$ was studied. For $\Delta t = 0.025$, the streamlines are virtually the same for $\Delta\zeta = \frac{1}{4}\Delta t$ and $\frac{1}{8}\Delta t$, and the flow pattern is essentially that shown in figure 6, with one main eddy being swept downstream. However, for $\Delta t = 0.0125$, as $\Delta\zeta$ was decreased the disturbance to the flow became increasingly vigorous. In particular, for $\Delta\zeta = \frac{1}{2}\Delta t$ there were many eddies at $t = 1.375$, and the calculations failed to converge at $t = 1.4625$.

From the above it is clear that the numerical instability is related to both Δt and $\Delta\zeta$, even when its effect is nonlinear and beyond the scope of §3 (changes in Δy are not significant provided there are sufficient points near the wall). The increase in growth rate with decrease in step size is consistent with an LWR instability. Further, an examination of the instantaneous velocity profiles for $H = 2$, $\Delta\zeta = 0.05$, $\Delta t = 0.0125$, and $\Delta y = 0.1$ shows that for $t \gtrsim 0.625$ LWR modes are present somewhere in the flow on the downstream side of the hill, and that the numerical instability is

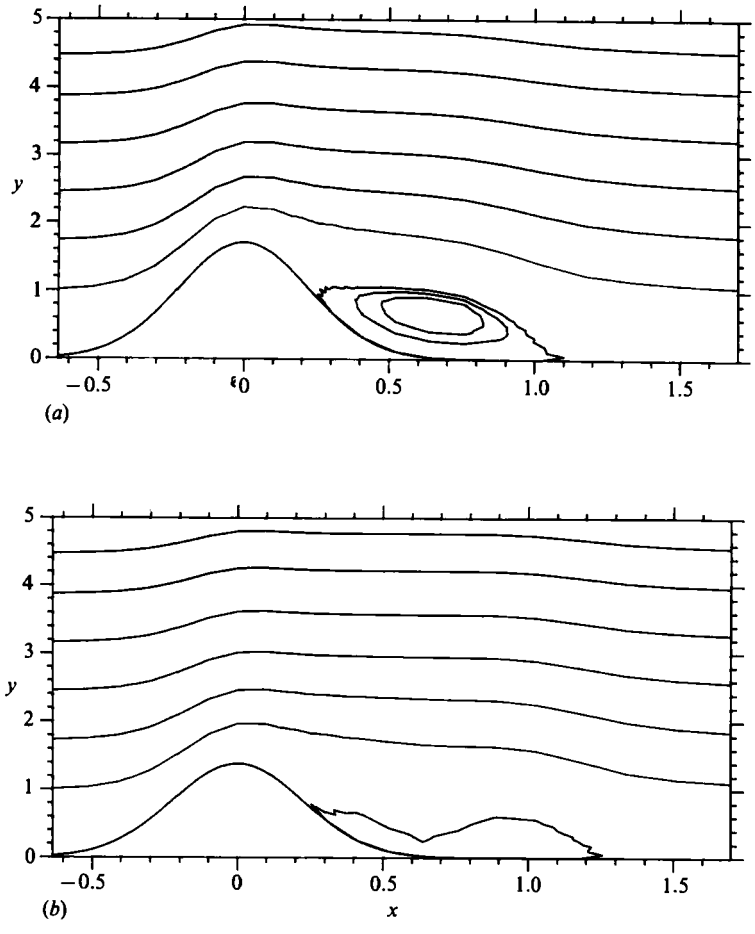

FIGURE 8. As for figure 7, but $\Delta\zeta = 0.10$.

strongest where the modes have their largest growth rate. For smaller values of H (e.g. $H = 0.6$) no instability was evident and no LWR modes could be found.

The dependence on step size makes it difficult to assess at what times the numerical results are reliable. For instance, the agreement between figures 6–8 at $t = 1.25$ is encouraging, but it is not conclusive because a sufficient decrease in step size for given rounding error can theoretically lead to the instability becoming order one at any fixed time after the LWR instability arises (see figure 10, and also §6).

Altering the frequency of the hill oscillation while holding the dimensions constant also affects the stability of the boundary-layer problem to LWR modes. In general, decreasing the frequency destabilizes the calculations by giving the unstable modes a greater opportunity to grow. In particular, for a very slowly oscillating hill the flow can be calculated to leading order as a sequence of quasi-steady problems, which were shown in §3 to be unstable if $h \gtrsim 0.7$. In contrast, increasing the frequency appears to stabilize the flow. For fast time variations Duck (1979) has shown that a two-layer asymptotic structure develops, consisting of an inviscid outer region and a Stokes layer at the wall. Although this flow has inflexion points, it does not admit LWR modes.

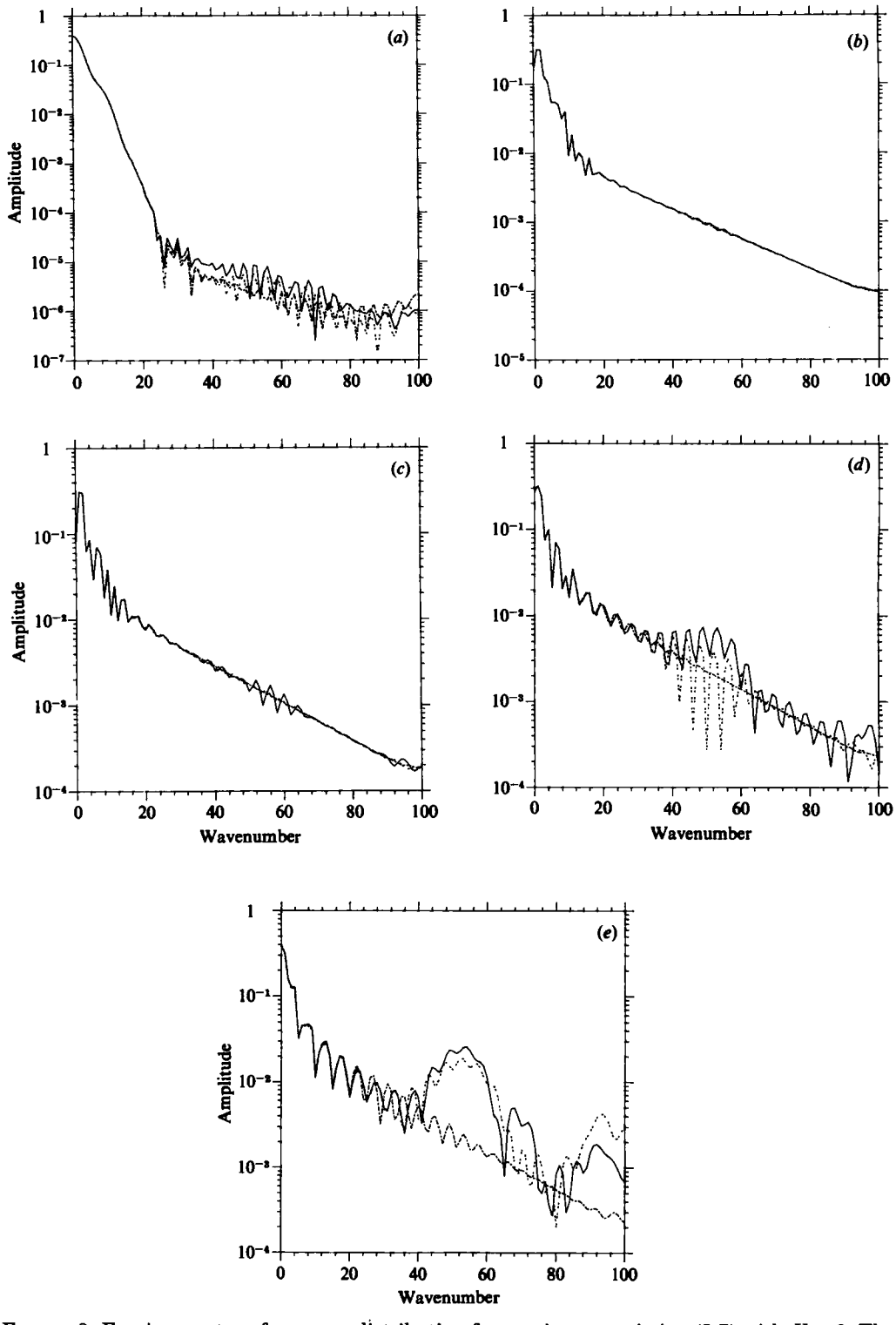

FIGURE 9. Fourier spectra of pressure distribution for moving constriction (3.7) with $H = 2$. The grid is $\Delta\zeta = 0.025$; $\Delta y = 0.1$; and -·-·-, $\Delta t = \Delta\zeta$; – – – – –, $\Delta t = \frac{1}{4}\Delta\zeta$; ——, $\Delta t = \frac{1}{16}\Delta\zeta$. (*a*) $t = 1.0$, (*b*) 1.125, (*c*) 1.25, (*d*) 1.375, (*e*) 1.5.

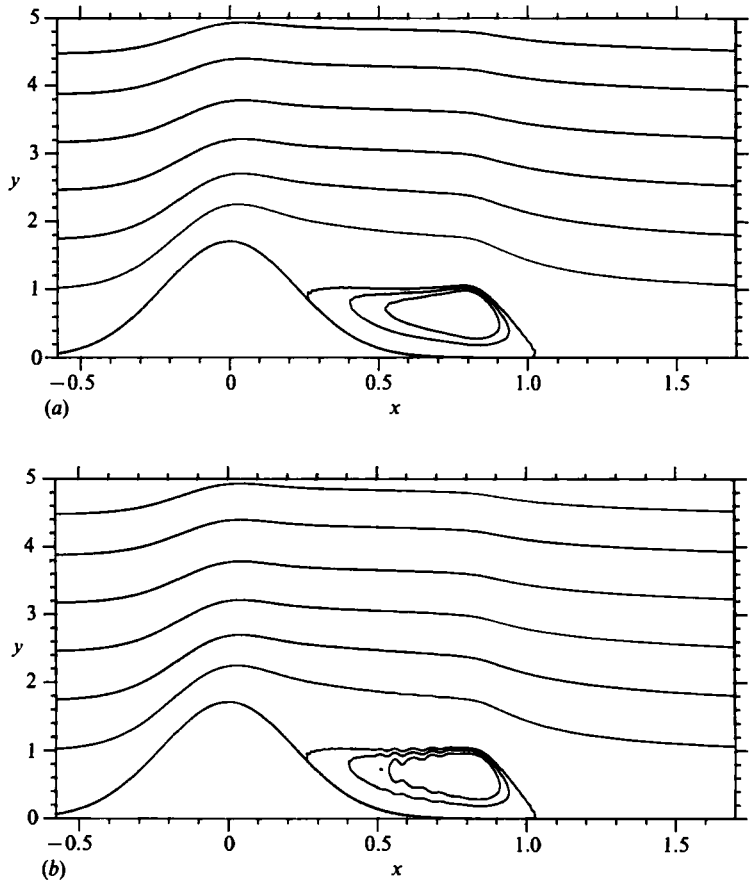

FIGURE 10. Streamline pattern for moving constriction (3.7) with $H = 2$ at $t = 1.25$. (a) $\Delta y = 0.1$, $\Delta\zeta = 0.006\,25$, $\Delta t = 0.025$; (b) $\Delta y = 0.1$, $\Delta\zeta = 0.003\,125$, $\Delta t = 0.0125$.

6. Discussion

Our principal conclusion is that the unsteady interactive formulation includes within it the mechanism for a long-wave Rayleigh instability. For interaction laws (2.4*a*, *b*, *e*, *f*, *h*) LWR modes can arise only if the streamwise velocity profile satisfies both Rayleigh's and Fjørtoft's theorems; although satisfaction of the latter theorem is not sufficient for the existence of either long-wavelength, or finite-wavelength, modes. For the hypersonic and Smith–Daniels (S–D) interaction laws we have been unable to show that either Rayleigh's or Fjørtoft's theorems apply to LWR modes. Indeed unstable velocity profiles can be constructed in S–D flow which do not include inflexion points (Appendix C).

The unsteady 'inverse' boundary-layer formulation also contains the LWR instability (with its consequent numerical difficulties). In this case Rayleigh's, but not Fjørtoft's, theorem has been recovered. For all the above formulations there are extensions of the instability analysis to three-dimensional flows, although these are not given here.

The effect of LWR modes on a numerical calculation was illustrated by solution of a problem describing flow through a slightly distorted channel. For sufficiently

large oscillation amplitudes of the distortion the flow generated became unstable to LWR modes. Once present, these modes resulted in the typical lengthscale of the motion decreasing, and made it difficult to obtain highly accurate finite-difference solutions; e.g. grid refinement tended to be counter-productive because it introduced shorter-wavelength more-rapidly-growing instabilities which resulted in truncation/rounding error growing to significance in a shorter time.

A similar loss of accuracy is encountered in the use of point-vortex methods to solve unsteady inviscid vortex sheet flows, e.g. increasing the number of point vortices can lead to an increasingly vigorous Kelvin–Helmholtz (K–H) instability (e.g. Moore 1981). This instability is acute because K–H modes, like LWR modes, have a growth rate that is directly proportional to the wavenumber α. Thus they have no fastest-growing mode and leave the problem ill-posed. In a numerical calculation, it is possible to 'control' the K–H instability to a certain extent either by spectral filtering or linear smoothing (Longuet-Higgins & Cokelet 1976; Moore 1981; Krasny 1986), and similar techniques may be successful here.

The physical mechanism which generates the LWR (or K–H) instability, and creates difficulties in a numerical calculation, is of course present in an 'exact' solution. In the case of vortex-sheet flows Moore (1979) has shown that if an initial disturbance has a Fourier transform that decays exponentially with increasing wavenumber, then as a result of the growth of K–H modes (i) the linear perturbation problem loses its analyticity after a finite time, and (ii) the full nonlinear flow can also develop a weak singularity in its vorticity distribution within a finite time.

Dr J. W. Elliott and Professor F. T. Smith (private communication 1984) have found instabilities similar to the above while studying marginally separated flows with an underlying velocity profile $u = y^2$. They show that, as in K–H flow, the linear disturbance problem can develop a finite-time singularity, and they surmize that a singularity develops in their nonlinear problem (see also Smith 1982*b*).

If the present instability is localized in space and consists only of LWR waves, then from (3.1) the linear perturbation velocity $\tilde{v} = v - v_0$ is

$$\tilde{v} \sim \int_{-\infty}^{\infty} \epsilon \mathscr{A}(x,t;\alpha) \exp\left(\mathrm{i}\Theta(X,T;\alpha)\right) \alpha \bar{v}(x,y,t;\alpha)\, \mathrm{d}\alpha, \tag{6.1}$$

where, for simplicity, $\Theta_X(X,0;\alpha) = 1$, $\mathscr{A}(x,0;\alpha) = g(\alpha)G(x)$, and $g(\alpha)$ is negligible when α is not large. The most straightforward case to consider is where the basic velocity profile and initial local wavenumber are both independent of x, so that $\Theta_X(X,T;\alpha) = 1$ from (3.1*c*). It then follows that if $g(\alpha)$ decays exponentially with α, a finite-time singularity develops in the *linear* solution (6.1) if $\mathrm{Im}\left(\int c\, \mathrm{d}t\right)$ becomes sufficiently large. By analogy with K–H flow, this suggests that it may be possible for the nonlinear solution to terminate in a singularity. Note that for a smooth distortion the exact solution does not become singular as soon as an LWR instability exists; although as the grid is refined, our numerical method fails in a shorter time. If the distortion's shape is such that the solution's Fourier spectrum decays algebraically with wavenumber, then (6.1) suggests that the solution may become singular almost as soon as LWR modes appear.†

† Many of the calculations were repeated for a distortion with $f(x,t) = h(t)\sin^3(\pi x)$, for $0 < x < 1$, and $f = 0$ elsewhere. The results were qualitatively the same as for the exponential hill (3.7), despite the algebraic decay of the Fourier transform of f. In particular, numerical solutions could be found well past the time at which LWR modes first appeared, although this may have been the result of using too coarse a grid.

If a singularity develops it will be necessary to consider asymptotic length and time scales other than those contained within the interactive boundary-layer formulation. However, an alternative way of modelling the flows in question might be to use the reduced Navier–Stokes equations suggested by Smith, Papageorgiou & Elliott (1984). This formulation, which includes finite-wavelength Rayleigh effects and thus the fastest-growing mode, may be singularity-free even if the interactive boundary-layer formulation is not.

In order to determine whether a nonlinear singularity can develop in the interactive formulation, the present finite-difference code would need refinement (e.g. by the introduction of spectral filtering); alternatively a full spectral code could be used (Duck 1985*a*). An improved code should also provide further information on the eddy splitting, some corroboration of which is given by the Navier–Stokes solutions of Belotserkovskii, Gushchin & Shchennikov (1975) for impulsively started flow past a circular cylinder. For $R \approx 1000$ the eddies in their solution (which is forced to be symmetric) do not settle down to a steady state but repeatedly divide. Also, we note that vortex shedding in a wall layer has been found in experimental studies of flow in constricted tubes (Cassanova & Giddens 1978; Ahmed & Giddens 1983).

Although our numerical results become unreliable before the initial eddy has divided completely, they are consistent with this effect being initiated by the LWR modes (§5). Consequently, it is possible that the eddy splitting observed by Stephanoff *et al.* (1983) is the finite-Reynolds-number manifestation of a Rayleigh instability. An alternative explanation of this phenomenon arises from including classical boundary layers in the inviscid analysis of Pedley & Stephanoff (1985). At sufficiently low oscillation frequencies the boundary-layer solution can terminate in a singularity, indicating that fluid is being ejected at a relatively large velocity from the boundary layer. This ejection may cause the eddy splitting.

The observation that velocity profiles with inflexion points exist for which no Rayleigh modes of any wavelength can be found (Appendix C and Smith & Bodonyi 1985), may be of potential relevance to the experiments of Klebanoff *et al.* (1962) and others on the 'spike' instabilities that occur in both boundary-layer and Poiseuille flow. Betchov (1960) and Greenspan & Benny (1963) proposed that the spike instability is an inflexion-point instability, and Nishioka, Asai & Iida (1980) found reasonably good agreement between experiment and an inviscid two-dimensional Rayleigh mode analysis. However, these theories do not fully explain why the spike instability is observed some time after the instantaneous velocity profiles satisfy Fjørtoft's criterion (which, in the case of classical boundary-layer velocity profiles, is normally a sufficient condition for instability). The reason for this may lie in the three-dimensionality and unsteadiness of the experiments. An alternative explanation may come from the application of the analysis above to free T–S waves described by the interactive boundary-layer equations. Such an unsteady analysis may demonstrate, in qualitative agreement with the experiments, that a Rayleigh instability develops only some time after Fjørtoft's criterion is satisfied.

Our final point is that there is the difficulty when constructing a theoretical model of a given observed flow of deciding which instabilities identified in an asymptotic analysis are relevant to a particular range of Reynolds numbers. In the case of *steady* solutions all unsteady instabilities are suppressed, and the asymptotic solution is assumed to be correct at large but stable Reynolds numbers.

The criterion for including/excluding instabilities in *unsteady* large Reynolds number asymptotics is less clear cut. In a system with random noise and a sufficiently

large Reynolds number, the most rapidly growing instability will be of most relevance. Alternatively, in a 'noise-free' forced flow, asymptotic scalings might be sought which either suppress all instabilities, or lead to the preferential excitation of others (for instance, insights into unsteady marginally separated flows have been obtained by suppressing the rapidly growing Rayleigh modes associated with the velocity profile's inflexion point, in favour of instabilities highlighted by interactive boundary-layer length and time scales). However, where instabilities have been scaled out of the problem and implicitly suppressed, careful justification seems necessary if a remaining asymptotic instability is said to describe an experimental observation.

In the case of the LWR modes identified above we suggest that they might be observable when a T–S instability is not, both because they have a faster growth rate than the T–S waves, and because the finite-Reynolds-number manifestations of Rayleigh instabilities tend to have lower critical Reynolds numbers than T–S-based instabilities (see for example the solutions of the Orr–Sommerfeld equations referred to by Drazin & Reid 1981).

However, it is not always expedient to suppress all but the fastest growing instability, or to favour Rayleigh modes. For example, Bodonyi, Smith & Gajjar (1983) and Smith & Bodonyi (1982) have studied the asymptotic structure of nonlinear upper-branch free T–S waves for both accelerating boundary-layer flow and Hagen–Poiseuille pipe flow. Both these studies include Stokes layers at the boundaries and nonlinear critical layers in the middle of the flow. However, the Stokes layers are unstable to Rayleigh modes over a typical time scale $O(R^{-\frac{1}{4}})$ (Cowley 1985), i.e. a time scale much shorter than the $O(1)$ period of the nonlinear T–S wave, while the work of Killworth & McIntyre (1985) suggests that the intermediate states through which the nonlinear critical layers will pass in attaining the assumed steady states may also be unstable to Rayleigh modes. Similarly, the Stokes layers generated by the high-frequency T–S waves studied by Smith & Burggraf (1985) are unstable to Rayleigh modes which have growth rates asymptotically larger than those of the T–S waves themselves (see also the rapidly growing Görtler instabilities found by Hall & Bennett (1986) for T–S waves propagating over a curved boundary).

The authors are grateful to Dr M. E. McIntyre for initially suggesting that an inviscid instability was responsible for the eddy splitting observed by Stephanoff *et al.* They are also grateful to Dr T. J. Pedley and Professor F. T. Smith for useful discussions, to the latter for revealing details of his work, and to the referees' for their helpful comments. O.R.T. thanks the SERC for financial support.

Appendix A. The stability of classical boundary-layer solutions

The aim of this Appendix is to demonstrate that solutions of the classical boundary-layer equation are unstable to rapidly growing asymptotic instabilities. To fix ideas the governing equations and boundary conditions for impulsively started flow past a circular cylinder are considered:

$$u_x + v_y = 0, \quad u_t + uu_x + vu_y = \sin x \cos x + u_{yy}, \tag{A 1a}$$

$$u = v = 0 \quad \text{on } y = 0; \quad u = 0 \quad \text{on } x = 0, \pi; \quad u \to \sin x \quad \text{as } y \to \infty. \tag{A 1b}$$

The solution to these equations on the forward face of the cylinder is unidirectional, while for $t \gtrsim 0.644$ reversed flow develops on the rearward face as the point of zero

wall shear x_0 moves upstream from $x = \pi$. At $t = t_s \approx 3.00$, $x = x_s \approx 1.93$ a singularity develops (van Dommelen & Shen 1980).

It is convenient to consider different sections of the cylinder's surface in turn:

(i) On the forward face of the cylinder, $u_y(y = 0) > 0$, $u_{yy}(y = 0) < 0$, and u increases monotonically with y. By application of the asymptotic description of T–S waves (e.g. Smith 1979*a*; Bodonyi & Smith 1981) it follows that linear disturbances with wavelengths between the lower- and upper-branch scalings, $O(R^{-\frac{3}{8}})$ and $O(R^{-\frac{5}{12}})$ respectively, have growth rates of $O(R^{\frac{1}{4}})$ where R is the Reynolds number based on cylinder diameter. Hence a multiple-scales argument formally demonstrates that the solution on the front of the cylinder is unstable.

(ii) On the whole of the reverse side of the cylinder there are inflexion points in the velocity profiles and Fjørtoft's criterion is satisfied. For $\frac{1}{2}\pi < x < x_0$ the velocity profiles are monotonic increasing functions of y, and hence Tollmien's (1936) heurisitic arguments suggest that Rayleigh modes with growth rates of $O(R^{\frac{1}{4}})$ will exist. These modes have fast growth rates and short wavelengths compared to the boundary-layer scales, and hence the classical boundary-layer solution is again formally unstable.

(iii) For the section of the rearward side $x_0 < x < \pi$, two types of mode exist. *First*, there is an unstable mode which has a lower branch with the T–S wavelength scale $O(R^{-\frac{3}{8}})$. Detailed calculations are necessary to determine whether this mode's upper branch is on the $O(R^{-\frac{1}{2}})$ Rayleigh lengthscale, or on the $O(R^{-\frac{5}{12}})$ T–S lengthscale (in the latter case the mode's asymptotic structure is slightly different from that known for a monotonic velocity profile because of the presence of two critical layers). Whatever the scale of the upper branch, this instability yields the classical boundary-layer solution formally unstable.

Secondly, there is a mode connected with the point of zero shear. Both the fastest growth rate and the upper branch of this mode occur on the $O(R^{-\frac{1}{2}})$ Rayleigh lengthscale. Its existence follows either from an asymptotic analysis of long-wavelength Rayleigh modes similar to that in Gill & Davey (1969), or from a short-wavelength stability analysis based on (A 1) (Cowley *et al.* 1985).

The above is not an extensive discussion, and special cases occur near $x = 0$, $\frac{1}{2}\pi$, x_0, π (see also Smith & Elliott 1985). Our aim has been to emphasize that the good agreement between classical boundary-layer theory and those large-Reynolds-number experiments which are apparently instability free (e.g. Bouard & Coutanceau 1980), is achieved by implicitly suppressing asymptotic instabilities.

Appendix B. The quadrature algorithm

The algorithm used to evaluate the contour integral $I = \int^y f(y')\,\mathrm{d}y'$ was based on a rational function (i.e. Padé) approximation of the integrand f. As usual the integration range was subdivided, and without loss of generality we consider the interval $(0, h)$. The subscripts 0, 1 are used to denote $y = 0, h$ respectively, and f_j, f'_j $(j = 0, 1)$ are assumed known.

The integrands of interest may include double-pole singularities, hence locally f is approximated by (cf. the more-usual Taylor series)

$$f(y) \sim \frac{e}{(1+dy)^2} + \frac{g}{(1+dy)} + k. \tag{B 1}$$

This approximation is a logical extension of Corkill & Stewart's (1983) work on the numerical solution of singular general relativity problems (see also their references).

Substituting (B 1) into the integral, and expressing the undetermined constants in terms of the f_j, f_j', we obtain

$$I_1 - I_0 \approx \frac{edh\,(2+dh)}{(1+dh)^2} + gd^{-1}\log(1+dh) + kh, \tag{B 2a}$$

$$k = f_0 - e - g, \quad g = -(2e + d^{-1}f_0'), \quad 2ed^2h = (1+dh)^2 f_1' - (1+dh)f_0', \tag{B 2b}$$

$$(1+dh) = \frac{f_1 - f_0 \pm \{(f_1-f_0)^2 - h^2 f_1' f_0'\}^{\frac{1}{2}}}{hf_1'}. \tag{B 2c}$$

The only significant difficulty with this method is in choosing the appropriate sign for the square root in (B 2*c*). Our algorithm chose the sign that yielded the least change in the predicted position of the singularity between (B 2*c*), i.e. $-d^{-1}$, and the equivalent expression for the sub-ranges $(-h, 0)$ or $(h, 2h)$. This choice is at least appropriate when the integrand is of the form (B 1).

The above integration scheme is relatively expensive computationally, and fails if f_j' is small. Hence over part of the integration range the 'cheaper' corrected trapezoidal rule was used. The choice of scheme depended on the local value of $s = f_0'^2/f_0 f_0''$. Near a double (single) pole $s \approx \frac{2}{3}$ $(\frac{1}{2})$ respectively. The Padé scheme was employed for $s_L \leqslant s \leqslant s_U$, where typically $s_L = 0.25$, $s_U = 0.95$; although s_U was varied on occasion to aid convergence of the secant iteration (see §3). We estimated s by assuming that locally $f \sim a(1+dy)^b$; then by elimination of a, b and d,

$$s \approx \frac{hf_0'f_1'}{hf_0'f_1' - f_1f_0' + f_0f_1'}. \tag{B 3}$$

The Padé approximation is formally $O(h^2)$ accurate, while the corrected trapezoidal rule is $O(h^4)$. Hence within their respective ranges of validity either algorithm is more than adequate, because the integrand itself is a numerical solution and only known to $O(h^2)$. Checks on the accuracy of the algorithm have been made; for example (B 1) can be integrated extremely accurately through a singularity on the real axis.

Appendix C. LWR instability of hypersonic and Smith–Daniels flow

For hypersonic and Smith–Daniels flow the standard proof of Rayleigh's and Fjørtoft's theorems fails because, from (3.2)–(3.5), $\bar{v} \to is\bar{p}K(y + A_0 - c) - i\bar{p}K$ as $y \to \infty$. Thus, for $s \neq 0$, the right-hand side of (3.8) becomes unbounded as $y \to \infty$. However, by rearranging (3.8) we obtain

$$\int_0^\infty \left(|\bar{v}_y - is\bar{p}K|^2 + \frac{u_{0yy}(u_0 - c^*)|\bar{v}|^2}{|u_0 - c|^2} \right) \mathrm{d}y = s|\bar{p}K|^2(1 + s(c - A_0)). \tag{C 1}$$

A modification of Rayleigh's theorem follows by taking the imaginary part of (C 1), viz. if $\mathrm{Im}\,(c) \neq 0$, then $u_{0yy} > 0$ somewhere in the flow. The real part of (C 1) appears to yield no generalization of Fjørtoft's theorem.

For Smith–Daniels flow, the existence of LWR modes can be illustrated by considering velocity profiles with $u_0 = y + u_1$, where $|u_1| \ll 1$. Then from (3.6)

$$c - 1 \sim \int_0^\infty \frac{u_{1y}}{(y-1)^2}\,\mathrm{d}y, \tag{C 2}$$

where the integration contour is to be deformed beneath/above $y = 1$ according as $\mathrm{Im}\,(c) \gtrless 0$. The integral can be evaluated consistently, and hence LWR modes exist, if $u_1''(1) > 0$ (note that there is *no* inflexion-point condition).

No equivalent demonstration of the existence LWR modes for hypersonic flow has been found, although for both hypersonic and Smith–Daniels flows continuous piecewise-linear velocity profiles can readily be constructed which admit LWR modes.

Appendix D. LWR instability of inverse boundary-layer solutions

In this Appendix the stability of inverse boundary-layer solutions to LWR disturbances is considered. Perturbations of the form (3.1a) and

$$U = U_0(x,t) + \epsilon \mathscr{A}(x,t) \exp\ (\mathrm{i}\Theta(X,T))\, \overline{U}(x,t), \tag{D 1}$$

are studied. Substitution into (2.1a, b) and (3.10) yields

$$-(u_0-c)\,\overline{v}_y + \overline{v} u_{0y} = -(U_0-c)\ \overline{V}', \tag{D 2a}$$

$$\overline{v} = 0 \quad \text{on } y = 0, \quad \overline{v}_y \to \overline{V}' \quad \text{as } y \to \infty, \tag{D 2b}$$

$$\int_0^\infty (U_0 \overline{v}_y - u_0 \overline{V}')\,\mathrm{d}y = 0. \tag{D 2c}$$

Solution of (D 2) results in the eigenvalue relation (assuming $\overline{V}' \neq 0$)

$$\delta = \int_0^\infty \left(1 - \left(\frac{U_0-c}{u_0-c^2}\right)^2\right)\mathrm{d}y. \tag{D 3}$$

Also $\overline{v} \to \overline{V}'(y-\delta)$ as $y \to \infty$, and hence in the limit $y \to \infty$ (3.8) becomes

$$\int_0^\infty \left(|\overline{v}_y - \overline{V}'|^2 + \frac{u_{0yy}(u_0-c^*)|\overline{v}|^2}{|u_0-c|^2}\right)\mathrm{d}y = |\overline{V}'|^2 \delta. \tag{D 4}$$

Rayleigh's inflexion-point theorem follows from taking the imaginary part of (D 4), while after minimal manipulation the real part yields

$$\int_0^\infty \frac{u_{0yy}(u_0-u_0(y_s))|\overline{v}|^2}{|u_0-c|^2}\mathrm{d}y = -\int_0^\infty |\overline{v}_y - \overline{V}'|^2\,\mathrm{d}y + |\overline{V}'|^2\,\delta, \tag{D 5}$$

where $u_{0yy}(y_s) = 0$. It follows that Fjørtoft's theorem holds where $\delta < 0$, but that the theorem might be violated where $\delta > 0$.

Numerical solutions for u_0 have not been substituted into the eigenvalue relation (D 3). However, unstable LWR modes have been found for model piecewise-linear velocity profiles with $\delta > 0$ and either a slight velocity overshoot or significant reversed flow.

REFERENCES

Ahmed, S. A. & Giddens, D. P. 1983 Velocity measurements in steady flow through axisymmetric stenoses at moderate Reynolds numbers. *J. Biomech.* **16**, 505–516.

Belotserkovskii, O. M., Gushchin, V. A. & Shchennikov, V. V. 1975 Use of the splitting method to solve problems of the dynamics of a viscous incompressible fluid. *Zh. vychisl. Mat. mat. Fiz.* **15**, 197–207.

Benjamin, T. B. 1961 The development of three-dimensional disturbances in an unstable film of liquid flowing down an inclined plane. *J. Fluid Mech.* **10**, 401–419.

Betchov, R. 1960 On the mechanisms of turbulent transition. *Phys. Fluids* **3**, 1026–1027.

Bodonyi, R. J. & Smith, F. T. 1981 The upper branch stability of the Blasius boundary layer, including non-parallel flow effects. *Proc. R. Soc. Lond.* A **375**, 65–92.

Bodonyi, R. J., Smith, F. T. & Gajjar, J. 1983 Amplitude-dependent stability of a boundary layer flow with a strongly non-linear critical layer. *IMA J. Appl. Maths* **30**, 1–19.

BOGDANOVA, E. V. & RYZHOV, O. S. 1983 The free and induced oscillations in the Poiseuille flow. *Q. J. Mech. Appl. Maths* **36**, 271–287.

BOUARD, R. & COUTANCEAU, M. 1980 The early stage of development of the wake behind an impulsively started cylinder for $40 < Re < 10^4$. *J. Fluid Mech.* **101**, 583–607.

BRADSHAW, P., CEBECI, T. & WHITELAW, J. H. 1981 *Engineering Calculation Methods for Turbulent Flow.* Academic.

BURGGRAF, O. R. & DUCK, P. W. 1982 Spectral computation of triple-deck flows. In *Numerical and Physical Aspects of Aerodynamic Flows* (ed. T. Cebeci). Springer.

CASSANOVA, R. A. & GIDDENS, D. P. 1978 Disorder distal to modelled stenoses in steady and pulsatile flow. *J. Biomech.* **11**, 441–453.

CEBECI, T. 1979 The laminar boundary layer on a circular cylinder started impulsively from rest. *J. Comp. Phys.* **31**, 153–172.

CEBECI, T. 1983 A time-dependent approach for calculating steady inverse boundary layer flows with separation. *Proc. R. Soc. Lond.* A **389**, 171–178.

CORKILL, R. W. & STEWART, J. M. 1983 Numerical relativity. II. Numerical methods for the characteristic initial value problem and the evolution of the vacuum field equations for space-times with two Killing vectors. *Proc. R. Soc. Lond.* A **386**, 373–391.

COWLEY, S. J. 1985 High frequency Rayleigh instability of Stokes layers. In *Proc. ICASE Workshop on the Stability of Time Dependent and Spatially Varying Flows.* To be published.

COWLEY, S. J., HOCKING, L. M. & TUTTY, O. R. 1985 On the stability of solutions of the unsteady classical boundary-layer equation. *Phys. Fluids* **28**, 441–443.

DENNIS, S. C. R. & SMITH, F. T. 1980 Steady flow through a channel with a symmetrical constriction in the form of a step. *Proc. R. Soc. Lond.* A **372**, 393–414.

DIJKSTRA, D. 1979 Separating, incompressible, laminar boundary layer flow over a smooth step of small height. In *Proc. 6th Intl Conf. Num. Meth. Fluid Dyn.* Springer.

DRAZIN, P. G. & REID, W. H. 1981 *Hydrodynamic Stability.* Cambridge University Press.

DUCK, P. W. 1979 Viscous flow through unsteady symmetric channels. *J. Fluid Mech.* **95**, 635–653.

DUCK, P. W. 1985*a* Laminar flow over unsteady humps: the formation of growing waves. *J. Fluid Mech.* **160**, 465–498.

DUCK, P. W. 1985*b* Pulsatile flow through constricted or dilated channels: Part II. *Q. J. Mech. Appl. Maths* **38**, 621–653.

GAJJAR, J. & SMITH, F. T. 1983 On hypersonic self induced separation, hydraulic jumps and boundary layers with algebraic growth. *Mathematika* **30**, 77–93.

GILL, A. E. & DAVEY, A. 1969 Instabilities of a buoyancy driven system. *J. Fluid Mech.* **35**, 775–798.

GREENSPAN, H. P. & BENNY, D. J. 1963 On shear-layer instability, breakdown and transition. *J. Fluid Mech.* **15**, 133–153.

HALL, P. & BENNETT, J. 1986 Taylor–Görtler instabilities of Tollmien–Schlichting waves and other flows governed by the interactive boundary-layer equations. *J. Fluid Mech.* (to appear).

JOBE, C. E. & BURGGRAF, O. R. 1974 The numerical solution of the asymptotic equations of trailing edge flow. *Proc. R. Soc. Lond.* A **340**, 91–111.

KILLWORTH, P. D. & MCINTYRE, M. E. 1985 Do Rossby-wave critical-layers absorb, reflect or over-reflect? *J. Fluid Mech.* **161**, 449–491.

KLEBANOFF, P. S., TIDSTROM, K. D. & SARGENT, L. M. 1962 The three-dimensional nature of boundary-layer instability. *J. Fluid Mech.* **12**, 1–34.

KRASNY, R. 1986 A study of singularity formation in a vortex sheet by the point vortex approximation. *J. Fluid Mech.* (to appear).

LONGUET-HIGGINS, M. S. & COKELET, E. D. 1976 The deformation of steep surface waves on water. *Proc. R. Soc. Lond.* A **350**, 1–26.

MOORE, D. W. 1979 The spontaneous appearance of a singularity in the shape of an evolving vortex sheet. *Proc. R. Soc. Lond.* A **365**, 105–119.

MOORE, D. W. 1981 On the point vortex method. *SIAM J. Sci. Stat. Comput.* **2**, 65–84.

NISHIOKA, M., ASAI, M. & IIDA, S. 1980 An experimental investigation of the secondary instability. In *Laminar–Turbulent Transition* (ed. R. Eppler & H. Fasel). Springer.

PEDLEY, T. J. & STEPHANOFF, K. D. 1985 Flow along a channel with a time-dependent indentation in one wall: the generation of vorticity waves. *J. Fluid Mech.* **160**, 337–367.

RIZZETTA, D. P., BURGGRAF, O. R. & JENSON, R. 1978 Triple-deck solutions for viscous supersonic and hypersonic flow past corners. *J. Fluid Mech.* **89**, 535–552.

RUBAN, A. I. 1978 Numerical solution of the local asymptotic problem of the unsteady separation of a laminar boundary layer in a supersonic flow. *Zh. vychisl. Mat. mat. Fiz.* **18**, 1253–1265.

RYZHOV, O. S. & ZHUK, V. I. 1982 Stability and separation of freely interacting boundary layers. In *Proc. 7th Intl Conf. Num. Meth. Fluid Dyn.* Springer.

SECOMB, T. W. 1979 Flows in tubes and channels with indented and moving walls. Ph.D. thesis, University of Cambridge.

SMITH, F. T. 1974 Boundary layer flow near a discontinuity in wall conditions. *J. Inst. Maths Applics* **13**, 127–145.

SMITH, F. T. 1976*a* Flow through constricted or dilated pipes and channels, Parts 1 & 2. *Q. J. Mech. Appl. Maths* **29**, 343–364 & 365–376.

SMITH, F. T. 1976*b* Pipeflows distorted by non-symmetric indentation or branching. *Mathematika* **23**, 62–83.

SMITH, F. T. 1979*a* Instability of flow through pipes of general cross section: Parts I & II. *Mathematika* **26**, 187–210 & 211–223.

SMITH, F. T. 1979*b* On the non-parallel flow stability of the Blasius boundary layer. *Proc. R. Soc. Lond.* A **336**, 91–109.

SMITH, F. T. 1979*c* Nonlinear stability for boundary layers for disturbances of various sizes. *Proc. R. Soc. Lond.* A **368**, 573–589 (and corrections, 1980, A **371**, 439–440).

SMITH, F. T. 1982*a* On the high Reynolds number theory of laminar flows. *IMA J. Appl. Maths* **28**, 207–281.

SMITH, F. T. 1982*b* Concerning dynamic stall. *Aero. Quart.* Nov./Dec. 331–352.

SMITH, F. T. 1984 Concerning upstream influence in separating boundary layers and downstream influence in channel flow. *Q. J. Mech. Appl. Maths* **37**, 389–399.

SMITH, F. T. & BODONYI, R. J. 1982 Amplitude-dependent neutral modes in the Hagen–Poiseuille flow through a circular pipe. *Proc. R. Soc. Lond.* A **384**, 436–489.

SMITH, F. T. & BODONYI, R. J. 1985 On short-scale inviscid instabilities in flow past surface-mounted obstacles and other non-parallel motions. *Aero. J.* **89**, 205–212.

SMITH, F. T. & BURGGRAF, O. R. 1985 On the development of large-sized short-scaled disturbances in boundary layers. *Proc. R. Soc. Lond.* A **399**, 25–55.

SMITH, F. T. & DANIELS, P. G. 1981 Removal of Goldstein's singularity at separation in flow past obstacles in wall layers. *J. Fluid Mech.* **110**, 1–38.

SMITH, F. T. & ELLIOTT, J. W. 1985 On the abrupt turbulent reattachment downstream of leading-edge laminar separation. *Proc. R. Soc. Lond.* A **401**, 1–27.

SMITH, F. T., PAPAGEORGIOU, D. & ELLIOTT, J. W. 1984 An alternative approach to linear and nonlinear stability calculations at finite Reynolds numbers. *J. Fluid Mech.* **146**, 313–330.

SOBEY, I. J. 1980 On flow through furrowed channels. Part 1. Calculated flow patterns. *J. Fluid Mech.* **96**, 1–26.

STEPHANOFF, K. D., PEDLEY, T. J., LAWRENCE, C. J. & SECOMB, T. W. 1983 Fluid flow along a channel with an asymmetric oscillating constriction. *Nature* **305**, 692–695.

STEWARTSON, K. 1981 D'Alembert's Paradox. *SIAM Rev.* **23**, 308–343.

TOLLMIEN, W. 1936 General instability criterion of laminar velocity distributions. *Tech. Mem. Nat. Adv. Comm. Aero. Wash. No.* 792.

VAN DOMMELEN, L. L. & SHEN, S. F. 1980 The spontaneous generation of the singularity in a separating laminar boundary layer. *J. Comp. Phys.* **38**, 125–140.

VELDMAN, A. E. P. & DIJKSTRA, D. 1980 A fast method to solve incompressible boundary layer interaction problems. in *Proc. 7th Intl Conf. Num. Meth. Fluid Dyn.* Springer.